MNRAS 000, 1–14 (2020) Preprint 24 February 2021 Compiled using MNRAS LATEX style file v3.0

MRI-active inner regions of protoplanetary discs. II. Dependence on dust, disc and stellar parameters

Marija R. Jankovic,[1]★ Subhanjoy Mohanty,[1] James E. Owen[1] and Jonathan C. Tan[2,3]
[1]*Astrophysics Group, Imperial College London, Blackett Laboratory, Prince Consort Road, London SW7 2AZ, UK*
[2]*Dept. of Astronomy, University of Virginia, Charlottesville, Virginia 22904, USA*
[3]*Dept. of Space, Earth & Environment, Chalmers University of Technology, Gothenburg, Sweden*

Accepted XXX. Received YYY; in original form ZZZ

ABSTRACT

Close-in super-Earths are the most abundant exoplanets known. It has been hypothesized that they form in the inner regions of protoplanetary discs, out of the dust that may accumulate in these regions if the magneto-rotational instability (MRI) operates there. In Paper I we presented a viscous disc model which includes heating due to both irradiation and MRI-driven accretion; thermal and non-thermal ionization; dust opacities; and dust effects on ionization. We studied the inner gas disc structure for a set of fiducial disc, stellar and dust parameters. In this paper we examine how the inner disc structure varies with these parameters. For high accretion rates and small dust grains, we find that: (1) the main sources of ionization are thermal ionization and thermionic and ion emission; (2) the disc features a hot, well-ionized, high-viscosity inner region, and a local gas pressure maximum at the outer edge of this region, (in line with previous studies); and (3) an increase in the dust-to-gas ratio pushes the pressure maximum outwards. Consequently, dust can accumulate in such inner discs without suppressing the MRI, with the amount of accumulation depending on the viscosity in the MRI-dead regions. Conversely, for low accretion rates and large dust grains, we find that: (1) stellar X-rays become the main source of ionization; (2) the X-rays drive high MRI-viscosity throughout the disc; and (3) the pressure maximum ceases to exist. Hence, overall, if planets form in the inner disc, larger accretion rates (and thus younger disks) are favoured.

Key words: planets and satellites: formation – protoplanetary discs

1 INTRODUCTION

Exoplanet discoveries have shown that super-Earths, planets with radii of 1–4 $R_\oplus$ and orbital periods shorter than $\sim$ 100 days, are incredibly common (Fressin et al. 2013; Dressing & Charbonneau 2013, 2015; Mulders et al. 2018; Hsu et al. 2019). To form the solid cores of these planets requires more mass in solids than is expected to exist at short orbital periods in the initial phases of planet formation in protoplanetary discs (Raymond et al. 2008; Chiang & Laughlin 2013; Schlichting 2014; Raymond & Cossou 2014). Because of this, it has been proposed that the super-Earths form further away from the star, in regions where temperature in the protoplanetary disc decreases enough for the water ice to condense, which increases the total amount of solids. In this hypothesis, ice-rich planets migrate inwards, to their present orbits, through gravitational interactions with the disc (Terquem & Papaloizou 2007; Ogihara & Ida 2009; McNeil & Nelson 2010; Cossou et al. 2014; Izidoro et al. 2017, 2019; Bitsch et al. 2019). However, when compared against atmospheric evolution models, the observed radius distribution of the super-Earths is found to be consistent with super-Earth cores being rocky, with very little ice present (Owen & Wu 2017; Van Eylen et al. 2018; Wu 2019).

This possibly implies that the super-Earths form in the inner, hot regions of protoplanetary discs, near their present orbits. As noted above, it is not expected that these inner regions contain, initially, enough mass in solids to form the super-Earths. However, the inner disc can be enriched by pebbles from the outer disc (Hansen & Murray 2013; Boley & Ford 2013; Chatterjee & Tan 2014; Hu et al. 2018; Jankovic et al. 2019), as pebbles are prone to inwards radial drift due to gas drag (Weidenschilling 1977). It has been hypothesized (Chatterjee & Tan 2014) that the radial drift of pebbles could be stopped at a local gas pressure maximum in the inner disc. Over time the pressure maximum could accumulate enough material to form a super-Earth-sized planet.

A gas pressure maximum is expected to form in an inner disc that accretes viscously via turbulence induced by the magneto-rotational instability (MRI; Balbus & Hawley 1991; Kretke et al. 2009; Dzyurkevich et al. 2010; Chatterjee & Tan 2014). The susceptibility of the disc to the MRI depends on the coupling between the gas and the magnetic field, and thus on the ionization fraction in

★ E-mail: m.jankovic16@imperial.ac.uk

the disc. In the hot innermost disc, the MRI is expected to drive high viscosity (i.e., efficient accretion) as a result of thermal ionization. At larger distances, where gas is colder and the ionization fraction drops, the viscosity is expected to be low (such a region is called a dead zone; Gammie 1996). In steady-state, a local gas pressure maximum forms at the transition between the high-viscosity and the low-viscosity regions (the dead zone inner edge).

The pressure maximum will only trap pebbles which are prone to radial drift relative to the gas. Smaller dust grains that are well coupled to the gas may be advected and diffused through the pressure maximum by the gas accreting onto the star. In the inner disc, the size of dust grains is limited by fragmentation due to relative turbulent velocities (Birnstiel et al. 2010, 2012; Drazkowska et al. 2016). Pebbles that radially drift from the outer to the inner disc become smaller due to fragmentation, and the effect of radial drift weakens. Jankovic et al. (2019) showed that, in an inner disc in which the gas accretion and the grain turbulent velocities are driven by the MRI, the grains can become small enough to escape the pressure trap, through advection and radial mixing by the turbulent gas. Additionally, it was found that this leads to an accumulation of small dust grains throughout the inner disc, interior to the pressure maximum.

Jankovic et al. (2019) did not explicitly take into account the effects of dust on the MRI, but that the accumulation of dust would quench the MRI in the innermost disc since dust grains are expected to quench the MRI by adsorbing free charges from the gas phase (Sano et al. 2000; Ilgner & Nelson 2006; Wardle 2007; Salmeron & Wardle 2008; Bai & Goodman 2009; Mohanty et al. 2013). As a consequence of quenching the MRI, the strength of the turbulence would fall allowing some grain growth. However, this would concurrently push the MRI-active region and the pressure maximum inwards, possibly eliminating it from the inner disc. Evidently, the outcome is a function of the size and the abundance of the dust grains.

In a companion paper (Jankovic et al. *submm.*; Paper I) we present a model of a steady-state viscously accreting disc which includes both the MRI-driven viscosity and the effects of dust on the MRI. This accounts for the adsorption of free charges onto dust grains, and also for the electron (thermionic) and ion emission from dust grains into the gas phase. The thermionic and ion emission become important at temperatures above $\sim$ 1000 K (so at the temperatures present in the inner disc) and act to increase the ionization fraction of the gas (Desch & Turner 2015). We find that for 1 μm grains, comprising 1% of the disc mass, these dust effects balance out and result in a pressure maximum at roughly the same location as predicted from thermal ionization. Additionally, this model also self-consistently considers the disc opacity due to dust grains, thus accounting for the effects of dust on the disc thermal structure.

In the above work, we focused on a fiducial disc model. Building on this, in this paper we investigate how the inner disc structure changes with dust-to-gas ratio, dust grain size, and other disc and stellar parameters, in order to narrow down the region of parameter space where the formation of planetary cores in the innder disc is more likely. We briefly overview our disc model in section 2 and present our results in section 3. In section 4 we focus on the existence and location of the gas pressure maximum as a function of the above parameters, exploring the entire parameter space in detail. In section 5 we discuss the implications of our results for the formation of the super-Earths and in section 6 we summarize our conclusions.

2 METHODS

Our disc model is presented in Paper I. Here, we only summarize the main points. It is assumed that the viscously-accreting disc is in steady-state, i.e., that the gas accretion rate $\dot{M}$ is radially constant. The disc structure is calculated self-consistently with disc opacities, ionization state and the viscosity due to the MRI. The disc is assumed to be in vertical hydrostatic and thermal equilibrium, heated by viscous dissipation and stellar irradiation, and cooled radiatively and/or via convection.

We consider disc opacities due to silicate dust grains, and we calculate the opacities for a MRN grain size distribution (Mathis et al. 1977), with a minimum grain size $a_{\rm min} = 0.1\,\mu$m and a maximum grain size $a_{\rm max}$, using optical constants from Draine (2003, see Paper I for details). Figure 1 shows the opacities per unit density of gas for different maximum grain sizes $a_{\rm max}$, assuming a dust-to-gas ratio $f_{\rm dg} = 0.01$, bulk density of dust grains $\rho_{\rm s} = 3.3\,{\rm g\,cm^{-3}}$, and stellar effective temperature $T_* = 4400\,$K. We only consider the structure of the disc beyond the silicate sublimation line, when dust opacities typically dominate over those of the gas, and so neglect the opacities due to gas molecular and atomic lines (but see section 5.3). Additionally, we neglect the contribution from the water ice and carbonaceous grains, since their sublimation temperatures are much lower than the temperatures expected in the hot MRI-active regions (e.g. Pollack et al. 1994).

The disc ionization state is calculated using a simple chemical network (Desch & Turner 2015) that includes thermal (collisional) ionization of potassium; ionization of molecular hydrogen by stellar X-rays, cosmic rays and radionuclides (producing metal (magnesium) ions by charge transfer); gas-phase recombinations; adsorption onto dust grains and thermionic and ion emission from dust grains. Only a single dust grain species of size $a_{\rm gr} = 0.1\,\mu$m is considered in the chemical network, but an effective dust-to-gas ratio $f_{\rm eff}$ is chosen to mimic the full size distribution stated above (see Paper I for details).

Finally, the viscosity due to the MRI, parametrized using the Shakura & Sunyaev (1973) α parameter, is calculated using a prescription based on the results of magnetohydrodynamic simulations (see Paper I). This accounts for the suppression of the MRI by Ohmic and ambipolar diffusion. In the MRI-dead zones (where the MRI is suppressed), we assume the gas can still accrete due to a small constant viscosity parameter $\alpha_{\rm DZ}$, induced either by the adjacent MRI-active zone or by purely hydrodynamical instabilities. The viscous α is calculated both as a function of radius and height, and we define a vertically-averaged viscosity parameter

$$\bar{\alpha} \equiv \frac{\int_0^{z_{\rm surf}} \alpha P dz}{\int_0^{z_{\rm surf}} P dz}, \tag{1}$$

where $z_{\rm surf}$ is the height of the disc surface, defined as the height the mid-plane where which the gas pressure falls below a small constant value of ????.

3 RESULTS

Here, we explore the effects of varying the important physical parameters on the inner disc structure. Initially, we vary the parameters one-by-one: dust-to-gas ratio $f_{\rm dg}$ and maximum dust grain size $a_{\rm max}$ in section 3.1, and the gas accretion rate $\dot{M}$, stellar mass M_*, and the dead-zone viscosity $\alpha_{\rm DZ}$ in section 3.2. We then extend the exploration of the parameter space by concurrently considering a larger dust grain size and a lower gas accretion rate, in section 3.3,

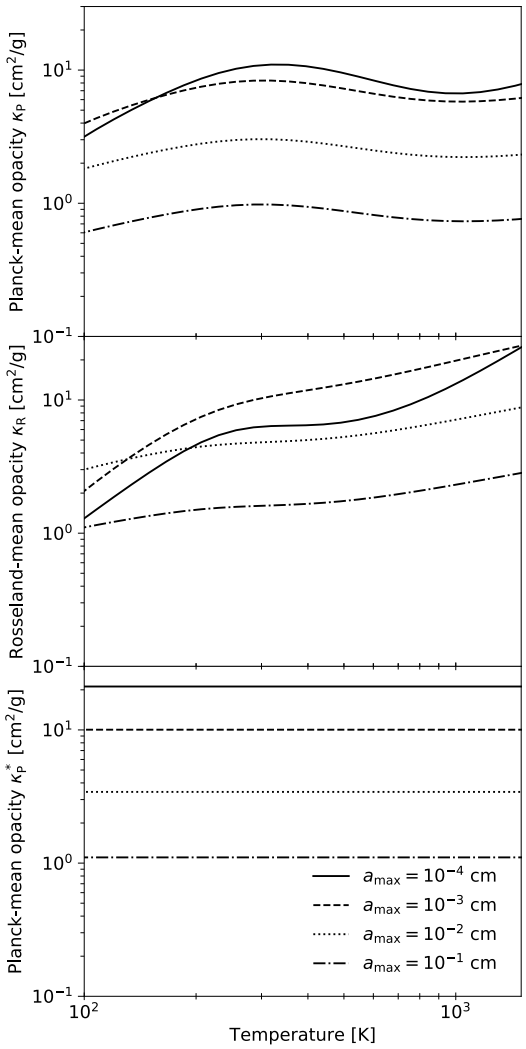

Figure 1. Planck-mean opacity κ_P (top), Rosseland-mean opacity κ_R (middle), and Planck-mean opacity at the stellar effective temperature κ_P^* (i.e., the absorption coefficient for the stellar irradiation; bottom), as functions of disc temperature, for different maximum grain sizes a_{max} as indicated in plot legend, assuming a dust-to-gas ratio $f_{dg} = 0.01$ and stellar effective temperature $T_* = 4400$ K. Absorption is dominated by small grains, and so the Planck-mean opacities decrease with increasing maximum grain size. The Rosseland-mean opacity is a non-monotonic function of grain size for $a_{max} \lesssim 10^{-2}$ cm.

discovering an X-ray dominated solution. As our fiducial model, taken from paper I, we consider a disc with a gas accretion rate $\dot{M} = 10^{-8}\,M_\odot\,yr^{-1}$, stellar mass $M_* = 1\,M_\odot$, stellar radius $R_* = 3\,R_\odot$, effective stellar temperature $T_* = 4400$ K[1], viscosity parameter in the MRI-dead zone $\alpha_{DZ} = 10^{-4}$, dust-to-gas ratio $f_{dg} = 10^{-2}$, and maximum dust grain size $a_{max} = 10^{-4}$ cm. In Paper I, this model was used to discuss the impact of various physical and chemical processes on the inner disc structure.

[1] These specific stellar parameters correspond to a Solar-mass star at an age of 0.5 Myr in the stellar evolution models of Baraffe et al. (2015). Over the first 5 Myr the luminosity of a Solar-mass star decreases by a factor of 5 in these models, and so the adopted parameters are roughly valid throughout the disc lifetime.

3.1 Dust-to-gas ratio and dust size

Dust has two effects on the disc structure in our model: it determines opacities in the disc, and it affects the disc ionization state. To better understand the results of varying dust properties, we first consider only the dust opacities. That is, in section 3.1.1, we consider a model with a vastly simplified chemical network, in which the only source of ionization is thermal ionization of potassium and free charges recombine only in the gas phase. Then, in section 3.1.2 we present the results of our full model which also accounts for the adsorption of charges onto dust grains, thermionic and ion emission from dust grains, and ionization of molecular hydrogen by stellar X-rays, cosmic rays and radionuclides.

3.1.1 Thermally-ionized model

In this section we consider a model which includes dust opacities, but does not include dust effects on the disc chemistry, nor ionization of molecular hydrogen. Ionization levels are exclusively set by thermal ionization. The results of varying the dust-to-gas ratio, f_{dg}, in the range $10^{-4} - 1$ are shown in the left column of Fig. 2.

In this simplified, thermally-ionized disc model, the MRI is active only at small radii. Therefore, the viscosity is highest in the innermost region where the midplane ionization fraction and the midplane temperature (shown in the second and third row, respectively) are highest, and it decreases with distance from the star. At some radius the ionization fraction drops below that needed to sustain the MRI, and the viscosity parameter $\bar{\alpha}$ falls to the minimum, dead-zone value α_{DZ}. That determines the location of the local gas pressure maximum, shown in the bottom panel.

We find that a higher dust-to-gas ratio results in a larger MRI-active zone (the region where $\bar{\alpha} > \alpha_{DZ}$). This is because the inner disc is optically-thick, so the disc midplane temperature is set by the accretion heat released near midplane and the optical depth of the disc to its own radiation (with a caveat that the vertical temperature gradient is additionally limited by convection; see Paper I). The disc's opacity is directly proportional to the dust-to-gas ratio, and so a disc with more dust is more optically-thick. This makes the midplane more ionized, leading to a higher MRI-induced viscosity at a given radius.

Furthermore, the right column of Fig. 2 shows models with a constant dust-to-gas ratio of $f_{dg} = 10^{-2}$, but varying the maximum dust grain size a_{max} in the range $10^{-4} - 1$ cm. For the three values of a_{max} considered here, the MRI-active region becomes smaller if dust grains are larger. This is because, for these values of a_{max}, larger dust grains have lower opacities (see Fig. 1), making the inner disc less optically thick. Just as in a disc with a lower dust-to-gas ratio, this makes the disc midplane cooler and less ionized. Going inwards, the MRI will become active roughly where the midplane temperature reaches ~ 1000 K, as necessary for the thermal ionization of potassium.

Therefore, in these simplified, thermally-ionized models, if dust growth were to happen, this would result in the MRI-active zone edge being pushed inwards. We emphasize that it is the changes to the dust opacities alone that lead to these significant changes in the

extent of the MRI-active zone. The effects of including dust grains in our chemical network are explored next.

3.1.2 *Full model*

In this section, we consider our full model that additionally includes (direct) effects of dust on the ionization fraction (adsorption of free charges onto dust grains, thermionic and ion emission), and also ionization of molecular hydrogen. Three sources of ionization are considered for the latter (stellar X-rays, cosmic rays and radionuclides), the X-rays being the most important (see Paper I). The results of varying the dust-to-gas ratio and maximum dust grain size in this full model are shown in the left and the right column of Fig. 3, respectively.

As in the simplified, thermally-ionized models discussed above, in the innermost regions the viscosity parameter decreases with distance from the star. Here, however, the viscosity parameter reaches a minimum value close to the dead-zone viscosity, and then increases again radially outwards, due to ionization by stellar X-rays (this is true in all models, even if not always evident in the plots). As discussed in Section 2 (Paper I; Desch & Turner 2015), in the full model the main source of ionization are thermionic and ion emission from dust grains in the inner disc. While this is fundamentally different mechanism from the gas-phase thermal ionization, due to similar activation energies, the ionization state of the disc are quantitatively similar. As a result, the viscosity parameter in these innermost regions is similar to the models with no dust. In Paper I, we discussed this for the fiducial maximum grain size $a_{\rm max} = 10^{-4}$ cm. The results presented in this work show that this conclusion holds at a wide range of dust-to-gas ratios and grain sizes (e.g., compare Fig. 3 with Fig. 2). Specifically, as highlighted in Section 2, the controlling physics of the ionization structure of an MRI accreting inner disc is thermionic and ion emission from dust grains for the majority of disc properties.

An exception to the above scenario is the case of high dust-to-gas ratio of $f_{\rm dg} = 1$. In this model, the midplane free electron fraction decreases substantially already at the distance of ~ 0.4 AU (see the left panel on the second row in Fig. 3). However, the viscous $\bar{\alpha}$ remains high out to ~ 2 AU in this model (the top left panel in Fig. 3). In this high-$\bar{\alpha}$ region, the MRI is indeed active at the disc midplane (as shown in the top panel of Fig. 4), despite the large decrease in the midplane electron number density. What drives the MRI in this case?

The bottom panel of Fig. 4 shows that between ~ 0.4 AU and ~ 2 AU the main ionized species are the potassium ions and the dust grains. As expected, the number density of electrons decreases with increasing dust-to-gas ratio (keeping other parameters fixed). However, the opposite is true for the number density of potassium ions evaporating from dust grains, above ~ 900 K (see Desch & Turner 2015), which must increase with increasing dust density. In the resulting disc ionization state, due to charge conservation, the total charge of potassium ions equals the total charge on dust grains. Clearly, since the dust grains have a much higher inertia than potassium ions, it is the potassium ions that couple the gas to the magnetic field. Overall, these results show that emission of potassium from dust grains is sufficient to sustain the MRI out to large radii, at high dust-to-gas ratios. Although, we not that at dust-to-gas ratios approaching unity the dynamical back reaction of the gas on the dust would need to be included, an effect which is poorly studied in the context of MRI turbulence and by extension not included in our parameterisation of the how the viscosity depends on the ionization structure. Clearly, MHD simulations of this disc state are warranted to study its behaviour.

Furthermore, as noted above, in our full model the viscosity parameter $\bar{\alpha}$ reaches a minimum value, outwards from which it increases with radius. The minimum in the viscosity parameter corresponds to the location of the gas pressure maximum, shown in the bottom panels of Fig. 3. Outwards of the pressure maximum, the temperature at the disc midplane is too low for efficient ionization, and so the MRI is only active in an X-ray-ionized layer high *above* disc midplane (seen near ~ 2 AU in the top panel of Fig. 4). In these outer regions, the viscosity parameter increases with decreasing dust-to-gas ratio and increasing dust grain size. This is because the main source of ionization are the stellar X-rays, and dust only acts as a recombination pathway. For lower dust-to-gas ratios and, equivalently, higher maximum grain size, the total grain surface area (onto which free charges adsorb) decreases, leading to higher ionization fraction and higher MRI-driven viscosity (Sano et al. 2000; Ilgner & Nelson 2006). Nevertheless, for the majority of the parameter space the contribution to the accretion rate from the X-ray-ionized layer is low in all cases and the viscosity parameter $\bar{\alpha} \sim \alpha_{\rm DZ}$ in this region. In other words, in these outer regions the gas primarily accretes through the dead zone, and the stellar X-rays do not affect strongly the location of the pressure maximum (for the given gas accretion rate).

Overall, the extent of the high-viscosity inner region and the location of the pressure maximum is dictated by the dependence of disc's vertical optical thickness on the dust-to-gas ratio and dust grain size through the effects discussed in the previous section. In our full model the location of the pressure maximum is approximately the same for $a_{\rm max} = 10^{-4}$ cm and $a_{\rm max} = 10^{-2}$ cm (see the top right panel in Fig. 3). This is because a larger grain size results in a lower effective dust-to-gas ratio in our chemical network. This slightly decreases the critical temperature at which the thermionic and ion emission make the gas sufficiently ionized to start the MRI at disc midplane. Concurrently, the decrease in the dust opacity with grain size is moderate for $a_{\rm max} \lesssim 10^{-2}$ cm (see Fig. 1). The location of the pressure maximum as a function of dust grain size is considered in more detail in section 4.

3.2 Gas accretion rate, stellar mass, dead-zone viscosity

In this section we keep the dust-to-gas ratio and the maximum dust grain size constant and equal to our fiducial values, and investigate how the structure of the inner disc changes with varying gas accretion rate, stellar mass and dead-zone viscosity. Fig. 5 shows the results of our fiducial model compared to three other models in which we vary these three parameters. The different panels show, from top to bottom, the vertically-averaged viscosity parameter ($\bar{\alpha}$), midplane free electron fraction ($n_{\rm e}/n_{\rm H_2}$), midplane temperature and midplane pressure, as functions of radius.

In each panel the dashed line shows a model with a gas accretion rate $\dot{M} = 10^{-9}\,{\rm M}_\odot\,{\rm yr}^{-1}$, lower than in our fiducial model with $\dot{M} = 10^{-8}\,{\rm M}_\odot\,{\rm yr}^{-1}$, shown by the solid line. The lower gas accretion rate results in a smaller high-viscosity inner region, and a gas pressure maximum at a shorter radius. This is because the gas accretion rate determines the total energy that is viscously dissipated (e.g. $T_{\rm eff}^4$, see Section 2) at any given radius. In the optically-thick inner disc, this sets the midplane temperature, the midplane ionization fraction and the viscosity. The radius of the gas pressure maximum scales with the gas accretion rate approximately as $r_{P\rm max} \propto \dot{M}^{1/2}$. This is, in fact, the same scaling previously found by Mohanty et al. (2018), who neglected heating by stellar irradiation, dust effects and

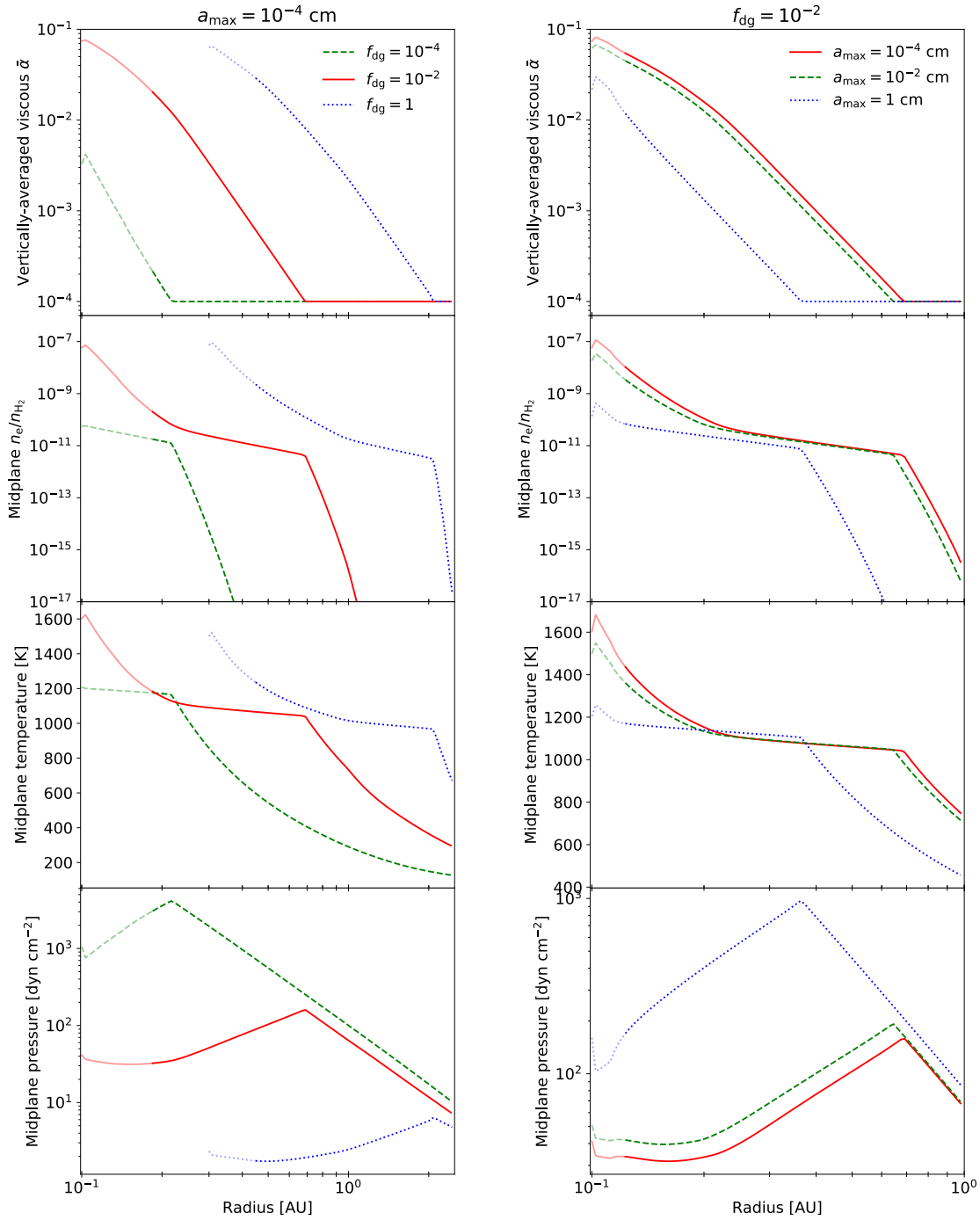

Figure 2. Results for a thermally-ionized disc (where the only source of ionization is thermal ionization of potassium, and dust effects on the disc chemistry are not included). The left column shows models with a constant maximum grain size $a_{\rm max} = 10^{-4}$ cm and varying dust-to-gas ratio $f_{\rm dg}$ as indicated in plot legend. The right column shows models with a constant dust-to-gas ratio $f_{\rm dg} = 10^{-2}$ and varying maximum grain size $a_{\rm max}$ as indicated in plot legend. The rows show radial profiles of (from top to bottom) vertically-averaged viscosity parameter $\bar{\alpha}$, midplane free electron fraction $n_{\rm e}/n_{\rm H_2}$, midplane temperature and midplane pressure. The inner edge of the $f_{\rm dg} = 1$ model is set to ~ 0.3 AU, since radially inwards temperature increases above the sublimation temperature of silicates. The light-coloured lines indicate the regions affected by the inner boundary condition (see Paper I). The radius of the pressure maximum is larger for a larger dust-to-gas ratio and a smaller maximum grain size. See Section 3.1.1.

6

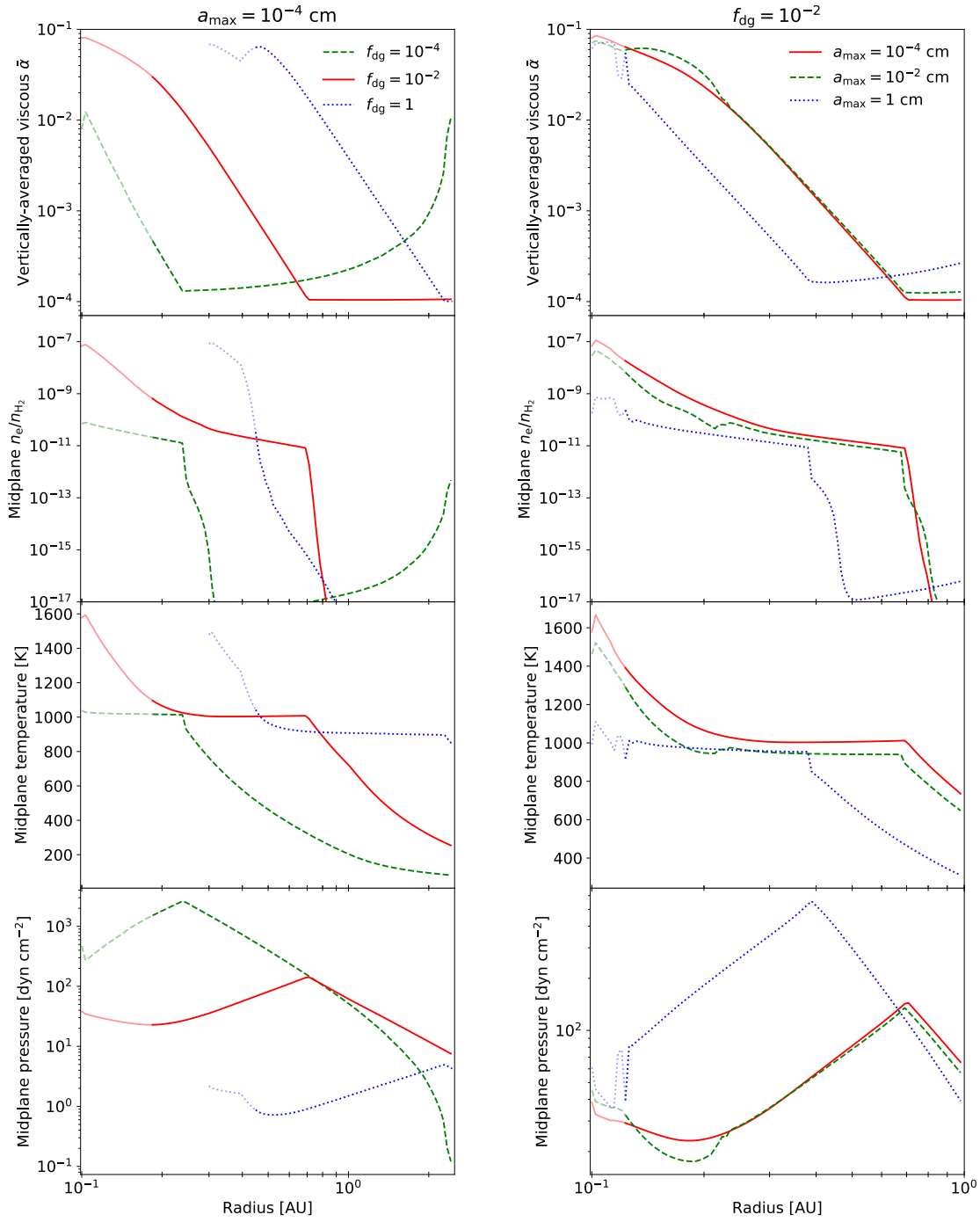

Figure 3. Results for our full model which includes dust effects on disc chemistry and ionization of molecular hydrogen. The left column shows models with a constant maximum grain size $a_{max} = 10^{-4}$ cm and varying dust-to-gas ratio f_{dg} as indicated in plot legend. The right column shows models with a constant dust-to-gas ratio $f_{dg} = 10^{-2}$ and varying maximum grain size a_{max} as indicated in plot legend. The rows show radial profiles of (from top to bottom) vertically-averaged viscosity parameter $\bar{\alpha}$, midplane free electron fraction n_e/n_{H_2}, midplane temperature and midplane pressure. The light-coloured lines indicate the regions affected by the inner boundary condition (see Paper I). The radius of the pressure maximum is larger for a larger dust-to-gas ratio; it is approximately the same for the maximum grain size of 10^{-4} cm and 10^{-2} cm, but quite smaller for the maximum grain size of 1 cm. See Section 3.1.2.

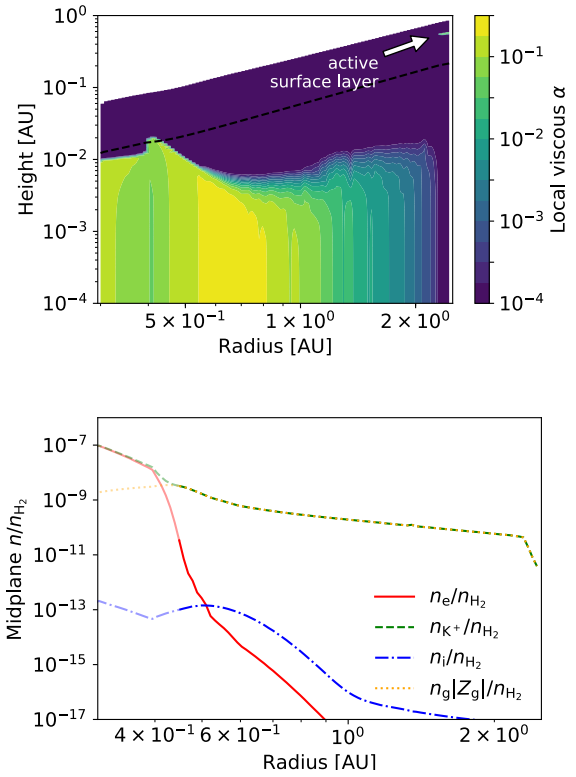

Figure 4. Local viscosity parameter α as a function of location in the disc (top) and the fractional number densities of various ionized species at the disc midplane as a function of radius (bottom), in a model with a dust-to-gas ratio of $f_{dg} = 1$ (with other parameters equal to the fiducial values). The species shown in the bottom panel are free electrons (n_e), potassium ions (n_{K+}), magnesium ions (n_i) and dust grains (n_g, carrying a mean charge Z_g). See Section 3.1.2.

ionization of molecular hydrogen. While we find that stellar irradiation and ionization of molecular hydrogen are indeed unimportant for the model parameters chosen here, the dust effects are not. However, while the chemistry setting the ionization state of the disc is qualitatively different in their simple models (thermal ionization of potassium) and in the models presented here (thermionic and ion emission), in both cases the ionization fraction increases sharply above roughly the same temperature (~ 1000 K), yielding the same approximate scaling.

X-ray ionization of molecular hydrogen becomes more important at the lower gas accretion rate. X-rays activate the MRI in a layer high above the disc midplane outwards of the pressure maximum, increasing the viscosity parameter $\bar{\alpha}$ compared to the dead-zone value α_{DZ}. For an accretion rate of 10^{-9} $M_\odot$ yr^{-1} the vertically averaged viscosity has increased by a factor of 2 outside the dead-zone over the model with an accretion rate of 10^{-8} $M_\odot$ yr^{-1}. This is because in these outer regions a lower gas accretion rate results in lower gas surface densities. Since the accretion rate carried by the X-ray ionized layer is roughly constant (e.g. set by the penetration depth of the X-rays) at lower accretion rates it has a larger relative contribution to the total the accretion rate. This contribution remains small for the small maximum grain size assumed here; in the next section we discuss how this finding changes if grains are larger.

We find that the structure of the inner disc surrounding a $M_* = 0.1\,M_\odot$ star[2] (shown by the dash-dotted lines in Fig. 5) is merely shifted radially inwards compared to our fiducial model with $M_* = 1\,M_\odot$. This is predominantly due to the dynamical (orbital) timescale being shorter at a given orbital radius around a less massive star, which reduces the total viscous dissipation at the given radius. The resulting approximate scaling $r_{P_{max}} \propto M_*^{-1/3}$ is consistent with the simple models of Mohanty et al. (2018), stressing again that (for the chosen $\dot{M}$, dust parameters etc.) stellar irradiation and ionization by stellar X-rays are unimportant in setting the location of the pressure maximum.

Finally, the dotted line in Fig. 5 shows a model with a dead-zone viscosity $\alpha_{DZ} = 10^{-3}$ (higher than our fiducial $\alpha_{DZ} = 10^{-4}$). As in the simple models of Mohanty et al. (2018), the exact value of α_{DZ} is unimportant in the innermost, well-ionized region. In the outer regions the accretion stress is dominated by that in the dead zone, and so α_{DZ} determines the minimum vertically-averaged viscosity parameter in the disc. Therefore, a larger α_{DZ} results in the pressure maximum moving radially inwards compared to the fiducial model.

3.3 Large dust grains and low accretion rates

Within the parameter space explored above, the steady-state solution for the inner disc structure remains qualitatively the same, with a local gas pressure maximum at the transition between the high-viscosity inner region and the low-viscosity outer region. Non-thermal sources of ionization (dominated by stellar X-rays) can suppress this picture by increasing the viscosity in the outer region and removing the pressure maximum. Within the parameter space explored above, the importance of non-thermal ionization increases for larger grains and lower gas accretion rates, but overall remains very small.

However, for large enough grains and low enough gas accretion rate, the steady-state solution can change qualitatively. We find that for a maximum grain size $a_{max} = 1$ cm and a gas accretion rate of $\dot{M} = 10^{-9}\,M_\odot\,\mathrm{yr}^{-1}$ (with other model parameters equal to the fiducial values) the viscosity parameter is of the order of $\bar{\alpha} \sim 0.1$ throughout the inner disc, and there is no local gas pressure maximum (see Fig. 6). In the bulk of the inner disc the metal ions vastly outnumber the potassium ions even at the disc midplane (Fig. 7), showing that non-thermal ionization is the main source of ionization in this solution.

4 PRESSURE MAXIMUM

The above results show that, for a wide range of disc, stellar and dust parameters, an MRI accreting protoplanetary disc features a high-viscosity inner region, a low-viscosity outer region, and a gas pressure maximum at the transition between the two regions. This gas pressure maximum has been hypothesized to have a key role in the formation of the super-Earths inside the water ice line (Chatterjee & Tan 2014). In this section, we wish to examine in more detail the existence and location of the pressure maximum.

[2] Here we adopt a stellar radius of $R_* = 1\,R_\odot$ and an effective temperature of $T_* = 2925$ K.

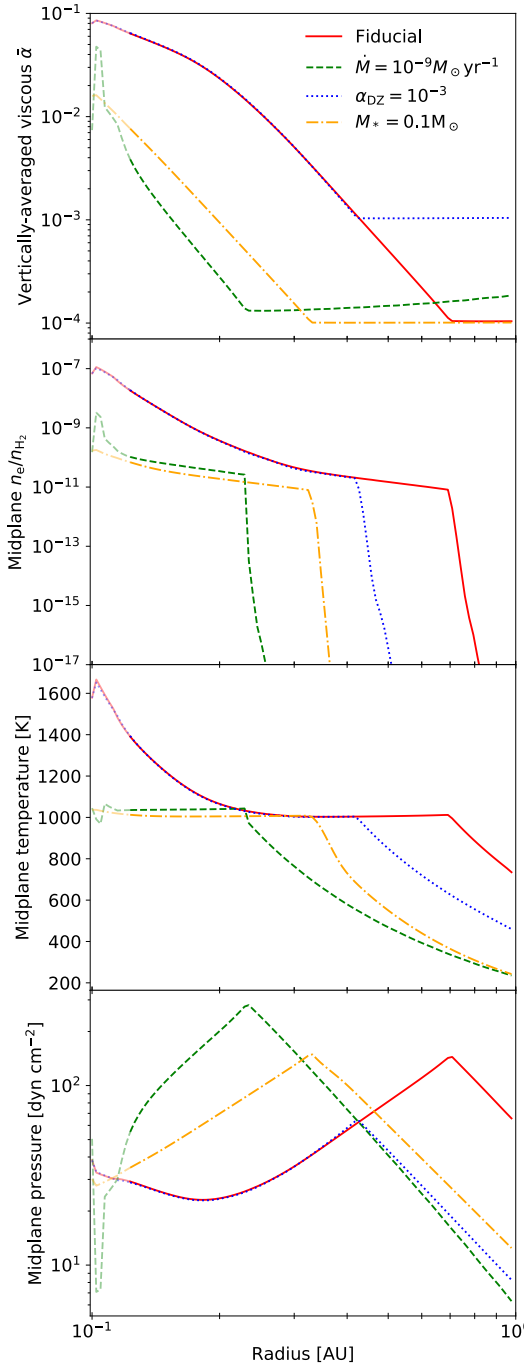

Figure 5. Results for our full model which includes dust effects on disc chemistry and ionization of molecular hydrogen. The different panels show radial profiles of (from top to bottom) vertically-averaged viscosity parameter $\bar{\alpha}$, midplane free electron fraction n_e/n_{H_2}, midplane temperature and midplane pressure. Fiducial model (solid lines) has a gas accretion rate $\dot{M} = 10^{-8}\,\mathrm{M}_\odot\,\mathrm{yr}^{-1}$, stellar mass $M_* = 1\,\mathrm{M}_\odot$ and dead-zone viscosity $\alpha_{\mathrm{DZ}} = 10^{-4}$. Models with a lower gas accretion rate (dashed line), a smaller stellar mass (dash-dotted line) or a larger dead-zone viscosity (dotted line) all yield the gas pressure maximum at a smaller radius. The light-coloured lines indicate the regions affected by the inner boundary condition (see Paper I). See Section 3.2.

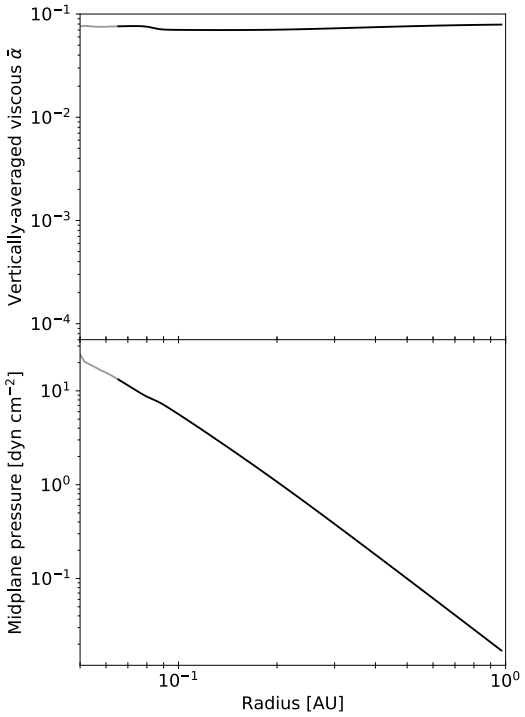

Figure 6. Vertically-averaged viscosity parameter $\bar{\alpha}$ (top) and midplane pressure (bottom) for a disc model with a gas accretion rate $\dot{M} = 10^{-9}\,\mathrm{M}_\odot\,\mathrm{yr}^{-1}$, stellar mass $M_* = 1\,\mathrm{M}_\odot$, dead-zone viscosity $\alpha_{\mathrm{DZ}} = 10^{-4}$, dust-to-gas ratio $f_{\mathrm{dg}} = 10^{-2}$ and maximum grain size $a_{\mathrm{max}} = 1\,\mathrm{cm}$. There is no local gas pressure maximum in the inner disc for these model parameters. The light-coloured lines indicate the regions affected by the inner boundary condition (see Paper I). See Section 3.3.

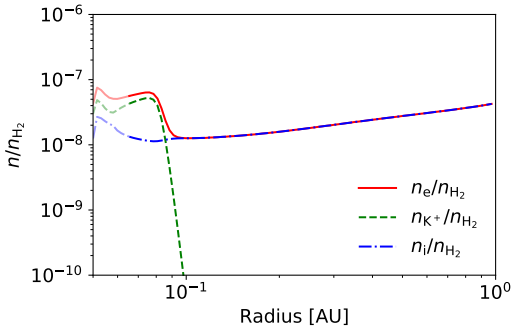

Figure 7. The fractional number densities of various ionized species at the disc midplane as a function of radius for the disc model shown in Fig. 6. The light-coloured lines indicate the regions affected by the inner boundary condition (see Paper I). See Section 3.3.

4.1 Existence of the pressure maximum

In section 3.3 we showed that a pressure maximum might be erased from the inner disc if there is a steady-state solution, for the given gas accretion rate, in which the stellar X-rays can become the primary source of ionization. Here, we are interested in exploring further in what parts of the parameter space this might occur. This requires us to reduce the computational complexity of the problem. We do this by choosing to neglect heating of the disc by stellar irradiation (but we still consider the ionization of the disc by the stellar X-rays).

This has been shown to be a good approximation if the inner disc is optically thick (see Paper I). For an optically-thick steady-state solution, including heating by stellar irradiation would only result in a minor quantitative change in the location of the pressure maximum. However, neglecting heating by stellar irradiation in the case of an optically-thin X-ray dominated solution can remove that solution altogether, leaving the optically-thick solution and incorrectly predicting that a pressure maximum should exist. This is because the temperature in a viscously-heated optically-thin disc is much lower than in an irradiation-heated disc, and so the accretion rates that can be attained through such solutions require higher column densities, and higher column densities lower the X-ray ionization rate at the disc midplane.

To account for these X-ray-dominated solutions, we proceed as follows. For a given set of disc and stellar parameters, we neglect the heating by stellar irradiation and find the radial location of the pressure maximum using our disc model. Then, we estimate the maximum gas accretion rate that can be attained in an irradiated X-ray-ionized disc, at that radial location. If this maximum gas accretion rate of an X-ray-dominated solution is larger than the given, input accretion rate, we assume that the pressure maximum would not exist in the inner disc for the given set of parameters. To estimate the maximum accretion rate in an irradiated X-ray-ionized disc, we assume the temperature equals the effective temperature due to stellar irradiation, and we adopt the flat-disc approximation for the incident angle of the irradiation. Furthermore, at low densities the important non-ideal MHD effect is ambipolar diffusion. The upper limit on the viscosity parameter α is imposed by the minimum plasma β parameter, $\beta_{\rm min}$, a function of the ambipolar Elsasser number Am (Bai & Stone 2011). Assuming that the only important charged species are electrons and atomic ions and that we are in the ambipolar-diffusion-dominated regime, Am $\approx n_{\rm i}\langle\sigma v\rangle_{\rm i}/\Omega$, where $n_{\rm i}$ is the number density of ions and $\langle\sigma v\rangle_{\rm i} = 1.6\times10^{-9}$ cm^3 s^{-1} is the rate coefficient for momentum transfer in collisions between ions and neutrals. We estimate Am and $n_{\rm i}$ at disc midplane, by assuming the only source of ionization are X-rays and atomic ions recombine on dust grains, using the reaction rates given in Paper I. In general, in our chemistry calculations we use an effective dust-to-gas ratio to mimic the grain size distribution; here we use the effective dust-to-gas ratio that corresponds to dust grains of different sizes being weighted by their surface area (different than in the rest of our calculations), which is a more appropriate choice when dust grains only act as a recombination pathway (see section 2.4.2 in Paper I).

Importantly, the number density of ions decreases with the gas surface density, due to attenuation of stellar X-rays. Because of this, the product of the viscosity parameter and the surface density, $\alpha\Sigma$, is maximized at some value of Σ, and so is the gas accretion rate (see Perez-Becker & Chiang 2011). Therefore, we can estimate the maximum gas accretion rate that can be obtained from an X-ray ionized optically-thin steady-state solution, and compare it to our assumed value.

4.2 Location of the pressure maximum

Fig. 8 shows the radial location of the pressure maximum (or pressure bump) as a function of the maximum dust grain size, for a stellar mass of 1 M$_\odot$ (the top panel) and 0.1 M$_\odot$ (the bottom panel). In all models shown here, we adopt our fiducial dust-to-gas ratio of 10^{-2}. The solid, dashed and dotted lines correspond to different values of the dead-zone viscosity parameter ($\alpha_{\rm DZ} = 10^{-5}$, 10^{-4} and 10^{-3}, respectively). For the different stellar masses we explore different ranges of the gas accretion rate $\dot{M}$, as indicated in plot legends next to each panel. The chosen ranges are motivated by observational studies, which find that for a Solar-mass star typically $\dot{M}\sim10^{-8}$ M$_\odot$ yr^{-1} and for the stellar mass of 0.1 M$_\odot$, typically $\dot{M}\sim10^{-10}$ M$_\odot$ yr^{-1} (e.g. Mohanty et al. 2005; Manara et al. 2012; Alcalá et al. 2014, 2017; Manara et al. 2017). There is a significant spread both in the reported mean values in these studies (±1 dex for the stellar mass of 0.1 M$_\odot$, and somewhat less for a Solar-mass star) and within the observed samples in each study (up to 2 dex). However, the correlation with the stellar mass appears robust, and so we adopt the above typical values as mean values and vary the gas accretion by ±1 dex for each stellar mass.

For the Solar-mass star we find that, for the upper end of the observed range of gas accretion rates ($\dot{M}\gtrsim10^{-8}$ M$_\odot$ yr^{-1}) and a wide range of $\alpha_{\rm DZ}$, the pressure maximum is found to exist at $r_{P_{\rm max}}\gtrsim0.1$ AU for a wide range of grain sizes. For the lower gas accretion rate ($\dot{M} = 10^{-9}$ M$_\odot$ yr^{-1}) and grain sizes larger than a few microns, the simple estimate described above suggests that a steady-state solution exists in which the disc is primarily heated by stellar irradiation and ionized by stellar X-rays. Therefore, we caution that a pressure maximum may not always occur for these parameters. For $M_* = 0.1$ M$_\odot$ the portion of the parameter space within which the pressure maximum is always present is even smaller, since the observed mean gas accretion rate is two orders of magnitude lower. Note that the range of grain sizes for which the pressure maximum exists for $\dot{M} = 10^{-9}$ M$_\odot$ yr^{-1} around the lower-mass star is larger than for the Solar mass star, due to the lower-mass star having a lower (X-ray) luminosity.

The radius of the pressure maximum as a function of the maximum dust grain size ($a_{\rm max}$) shows a similar trend across the various values of the stellar mass, accretion rate and dead-zone viscosity: it weakly increases with increasing $a_{\rm max}$ for small grains, peaks at about $a_{\rm max}\sim10^{-2}$ cm, and then steadily decreases for larger dust grains. The factors causing this have already been briefly discussed in section 3.1. First, recall that a increase in the disc opacity means that accretion heat can escape less easily, making the disc midplane hotter and pushing the pressure maximum outwards. In addition, for small dust grains, larger dust grain size leads to a moderate increase in the opacity (here, the relevant opacity is the opacity of the disc to its own radiation in the optically-thick regions, i.e., the Rosseland-mean opacity, see Fig. 1). At the same time, the increase in dust grain size reduces the critical temperature at which ionization fraction rises due to thermionic and ion emission (as the increase in dust grain size is equivalent to a reduction in the effective dust-to-gas ratio in our chemical network; see also Desch & Turner 2015), pushing the pressure maximum outwards. Concurrently, when X-ray ionization is important, the minimum value of the viscosity parameter is larger for larger grains, pushing the pressure maximum inwards. When all these factors are compounded, for small grains, the radius of the pressure maximum increases with $a_{\rm max}$. However, if the grains grow beyond $a_{\rm max}\sim10^{-2}$ cm, dust opacities are severely decrease with increasing grain size and the net effect is a decrease in the radius of the pressure maximum. Ad-

10

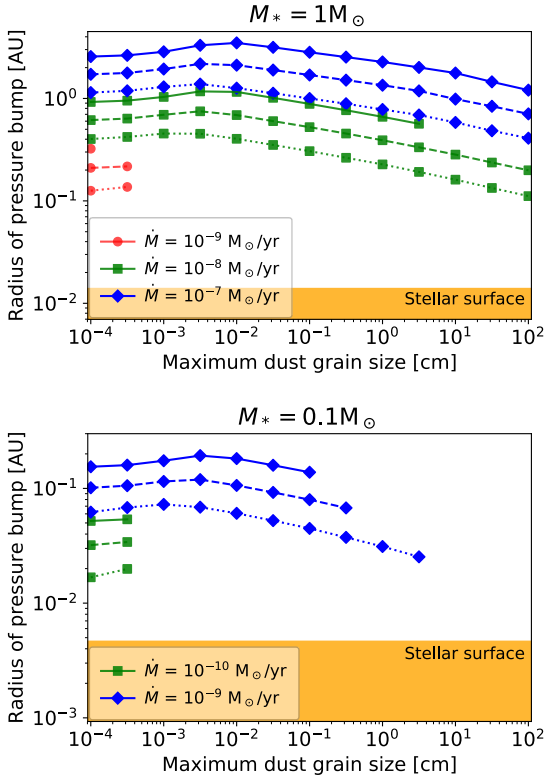

Figure 8. Radius of gas pressure bump as a function of maximum dust grain size. Top panel shows the results for a stellar mass $M_* = 1\,M_\odot$, bottom panel for $M_* = 0.1\,M_\odot$. In all models the dust-to-gas ratio is 10^{-2}. Solid, dashed and dotted lines show results for the dead-zone viscosity parameter $\alpha_{DZ} = 10^{-5}$, 10^{-4} and 10^{-3}, respectively. Blue, green and red lines indicate different gas accretion rates $\dot{M}$ as indicated in plot legends for each panel. To obtain these results, we neglect heating by stellar irradiation in our disc model, and use a simple calculation to estimate if including the irradiation would produce a steady-state solution ionized primarily by stellar X-rays and featuring no pressure maximum. This is indeed found to be the case for lower accretion rates and larger dust grains. For $M_* = 0.1\,M_\odot$, there is no pressure maximum for the lower end of the observed accretion rates ($\dot{M} = 10^{-11}\,M_\odot\,yr^{-1}$) for any maximum grain size. See Section 4.

ditionally, note that the exact value of a_{max} at which the radius of the pressure bump peaks varies somewhat with $\dot{M}$ and α_{DZ}; this can be expected, since both determine the gas surface density and thus the optical depth at disc midplane and the relative importance of the above three effects. It is also important to note that including heating due to stellar irradiation seems to somewhat modify the trend for small dust grains, as can be seen by comparing Fig 8 to the models discussed in the previous section (specifically, Fig. 3 shows that for our fiducial disc and stellar parameters, micron-size grains result in a pressure maximum at a larger radius. The resulting differences in the radial location of the pressure maximum are, however, small, and certainly for larger grains the pressure maximum moves inwards.

5 DISCUSSION

In this work we have investigated how the structure of the inner disc, accreting primarily through the MRI, changes with various disc, stellar and dust parameters. Of particular interest are the existence and the location of a local gas pressure maximum and a highly-turbulent region inwards of it, which could accumulate dust grains drifting in radially from the outer disc, possibly leading to the formation of planetary cores (Chatterjee & Tan 2014; Hu et al. 2018; Jankovic et al. 2019). The models presented in this work are steady-state models, each with a distribution of dust grains that is fixed throughout the disc. However, as discussed in the rest of this section, these models provide us with important insights into how the inner disc could evolve as the dust grains grow, if and how the dust will accumulate, how this accumulation could feedback on the gas structure, and the disc parameters that are favourable for the formation of planetary cores.

5.1 Dust growth

As discussed in Section 4.2 dust growth to $a_{max} \sim 10^{-2}$ cm increases the extent of the high-viscosity inner region and the radius at which the pressure maximum is located, as an increase in dust grain size leads to a moderate increase in the disc opacity and a decrease in the threshold temperature at which thermionic and ion emission become efficient. Growth beyond that size has the opposite effect, as it leads to a significant decrease in the disc opacity, making the disc midplane colder, and thus less ionized. Therefore, in the inner disc, if dust grows larger than $\sim 100\,\mu$m sizes, the dead-zone inner edge moves inwards.

Note that this is the opposite of what happens in the outer regions of protoplanetary discs. The outer regions are ionized primarily by the stellar X-rays and cosmic rays. These sources of ionization become more important further away from the star, as the disc column density decreases and high-temperature effects become unimportant. These regions are expected to be optically thin to their own radiation, and the primary source of heat is stellar irradiation. Therefore, the dust acts primarily to lower the ionization fraction by adsorbing free charges from the gas. Because of this, in the outer regions the dead zone is expected to shrink as the dust grains grow (Sano et al. 2000; Ilgner & Nelson 2006).

In the inner disc, dust growth is limited by collisional fragmentation of dust grains due to relative turbulent velocities (Birnstiel et al. 2010, 2012; Drazkowska et al. 2016). We wish to consider the location of the pressure maximum under the assumption that the maximum dust grain size has reached this limit, with the relative grain velocities induced by the MRI-driven turbulence. This limit is described in terms of the particles "Stokes number" (St, the ratio between the particle stopping time and the eddy turnover time, where the eddy turnover time is taken to be $1/\Omega$). In a turbulent disc, typical collisional relative velocity between dust grains is given by $V_{dd}^2 \approx 3V_g^2$St (for St < 1, Ormel & Cuzzi 2007), where V_g is the typical turbulent gas velocity (given by $V_g^2 = \alpha c_s^2$). There is a critical velocity u_{frag} above which a collision between dust grains results in their fragmentation, rather than sticking/growth. For silicate grains of similar size, $u_{frag} \sim 1\,m\,s^{-1}$ (Blum & Münch 1993; Beitz et al. 2011; Schräpler et al. 2012; Bukhari Syed et al. 2017, although note that grains might become more sticky at the high temperatures present in the inner disc Demirci et al. (2019)). Since the Stokes number St is directly related to the grain size, and the collision velocity to St, fragmentation imposes an upper limit on dust growth.

At the fragmentation limit (Birnstiel et al. 2009, 2012),

$$\mathrm{St}_{\mathrm{frag}} = \frac{u_{\mathrm{frag}}^2}{3\alpha c_{\mathrm{s}}^2}. \quad (2)$$

The exact relationship between the Stokes number and the particle size depends on the relevant drag law (Weidenschilling 1977). Typically, the dust grains in protoplanetary discs are smaller than the mean free path of gas molecules, and therefore couple to the gas according to the Epstein drag law. However, due to the high densities in the inner disc, dust grains may enter the Stokes regime. Importantly, the above approximate expression for the turbulent relative velocity between dust grains (V_{dd}) has been derived under an assumption that St does not depend on the relative velocity between the dust grain and the gas, V_{dg}. This assumption is true for grains in the Epstein drag regime. In the Stokes regime, it is true only if the Reynolds number Re of the particle is less than unity. We always check that this condition is fulfilled for our particles in the Stokes regime, and that we may employ the above expression for V_{dd}. The Reynolds number of a particle itself depends on the velocity V_{dg}, for which we adopt another approximate expression, $V_{\mathrm{dg}}^2 = V_{\mathrm{g}}^2 \mathrm{St}/(1 + \mathrm{St})$ (Cuzzi & Hogan 2003, note that this expression was derived analytically for $\mathrm{St} \ll 1$, but also shown to be applicable for a wide range of St through a comparison with numerical simulations).

To calculate the location of the pressure maximum in a disc in which grain growth is limited by fragmentation, we proceed as follows. At the location of the pressure maximum for various combinations of stellar mass, accretion rate, dead-zone viscosity parameter and maximum dust grain size (i.e., for every point in Fig. 8), we calculate the fragmentation limit for the particle Stokes number, $\mathrm{St}_{\mathrm{frag}}$ (assuming $\alpha = \bar{\alpha}$), and the corresponding grain size, a_{frag} (for an appropriate drag law). Then, for every combination of the stellar mass, accretion rate and dead-zone viscosity parameter, using linear interpolation, we find the grain size such that $a_{\mathrm{frag}}(a_{\mathrm{max}}) = a_{\mathrm{max}}$. This yields a corresponding radius of the pressure maximum.

Note that this calculation utilizes models in which the maximum dust grain size is assumed to be constant everywhere in the disc, and so the obtained solutions also formally correspond to models in which the maximum dust grain size is radially constant (and equal to the fragmentation limit a_{frag} at the pressure maximum). In a real disc, the fragmentation limit to which particles can grow would be a function of the turbulence levels and other parameters which vary as functions of radius. While this calculation does not take this radial variation of dust size into account, the fragmentation limit at the pressure maximum and the location of the pressure maximum would remain the same as in the solutions found here. In particular, note that radially inwards from the pressure maximum, a_{frag} should decrease compared to the value at the pressure maximum, as the turbulent strength increases. As we will find, the solution for a_{frag} at the pressure maximum is always higher than a_{max} at which the radius of the pressure maximum peaks (as a function of a_{max}, in Fig. 8). That is, at a fixed radius, a decrease in particle size inwards of the pressure maximum would yield an increase in the viscosity parameter, compared to the value calculated using the fragmentation limit at the pressure maximum. Accounting for the radial variation in particle size would then make the radial gradient of the viscosity parameter steeper inwards of the pressure maximum, but it would not change the location of its minimum, and therefore not the location of the pressure maximum obtained here.

The results for the radius of the pressure maximum and the grain size are shown in Fig. 9, as functions of the gas accretion rate, for different values of stellar mass and the dead-zone viscosity parameter. The maximum grain size at the pressure maximum is limited by turbulent fragmentation (middle panel) and thus sensitive to the dead-zone viscosity parameter α_{DZ} (results for $\alpha_{\mathrm{DZ}} = 10^{-5}$, 10^{-4} and 10^{-3} are shown by the solid, dashed and dotted lines, respectively). This is because the location of the pressure maximum corresponds to the location of the minimum in the vertically-averaged viscosity (and turbulence) parameter $\bar{\alpha}$.

Remarkably, despite the sensitivity of the grain size to α_{DZ}, the radius of the pressure maximum depends very weakly on this parameter. Basically, we find that the fragmentation-limited solution for the grain size is always larger than the grain size at which the radius of the pressure maximum peaks as a function of the grain size (see Fig. 8). Therefore, in this region of the parameter space, a larger grain size yields a smaller radius of the pressure bump. Larger (fragmentation-limited) grain size is obtained for lower values of the dead-zone viscosity parameter, as discussed above. Concurrently, at a fixed grain size (and other parameters), a lower dead-zone viscosity parameter yields a larger radius of the pressure bump (see Section 3.2). Evidently, compounding these inter-dependencies results in a weakly-varying radius of the pressure bump for a wide range of values for the dead-zone viscosity parameter.

Furethermore, for the Solar-mass star, the pressure maximum is located at radii $\gtrsim 0.1\,\mathrm{AU}$ in the upper end of the range of the observationally-motivated gas accretion rates considered here. Compounding this with our result that a higher dust-to-gas ratio (resulting from accumulation of dust, see also the next section) would move the pressure maximum outwards, this places the potentially planet-forming region within the range of the observed orbital distances of the super-Earths. However, for the accretion rate of $\dot{M} = 10^{-9}\,\mathrm{M}_{\odot}\,\mathrm{yr}^{-1}$ there may not be a pressuer maximum. As discussed in Section 4, for lower gas accretion rates and larger dust grain sizes, we find that the disc could assume a high-viscosity X-ray-dominated steady-state solution which features no pressure maximum.

For a lower-mass star, $M_* = 0.1\,\mathrm{M}_{\odot}$, at a fixed gas accretion rate, dust grains may grow to somewhat larger sizes than for the Solar-mass star. Overall, the radius of the pressure maximum is expected to be smaller, due to the larger grain sizes, but also (mostly) due to the lower viscous dissipation rate and the lower observed gas accretion rates (see the discussions in sections 3.2 and 4). Analogously to the case of the Solar-mass star, there might not be a pressure maximum at lower accretion rates.

5.2 Dust accumulation

For dust grains to become trapped within the pressure maximum, the outwards radial drift velocity of dust grains just inwards of the pressure maximum should be higher than the velocity with which the accreting gas advects the grains inwards. The ratio of the radial drift and the gas advection velocities is roughly equal to the ratio of the particle Stokes number and the viscous α (Jacquet et al. 2012). Therefore, for the particle radial drift to overcome advection with the gas inwards of the pressure maximum, it is required that $\mathrm{St}/\alpha > 1$. To check whether this condition is fulfilled, in the bottom panel of Fig. 9 we show the ratio between the Stokes number at the fragmentation limit $\mathrm{St}_{\mathrm{frag}}$ and the viscosity and the vertically averaged turbulence parameter $\bar{\alpha}$.

The ratio $\mathrm{St}_{\mathrm{frag}}/\bar{\alpha}$ is most sensitive to the value of the dead-zone viscosity parameter α_{DZ}. The Stokes number at the fragmentation limit $\mathrm{St}_{\mathrm{frag}}$ is given by eq. (2). At a fixed critical fragmentation velocity u_{frag}, it is a function only of the viscosity parameter $\bar{\alpha}$ and the speed of sound c_{s} (i.e., the temperature) at the pressure

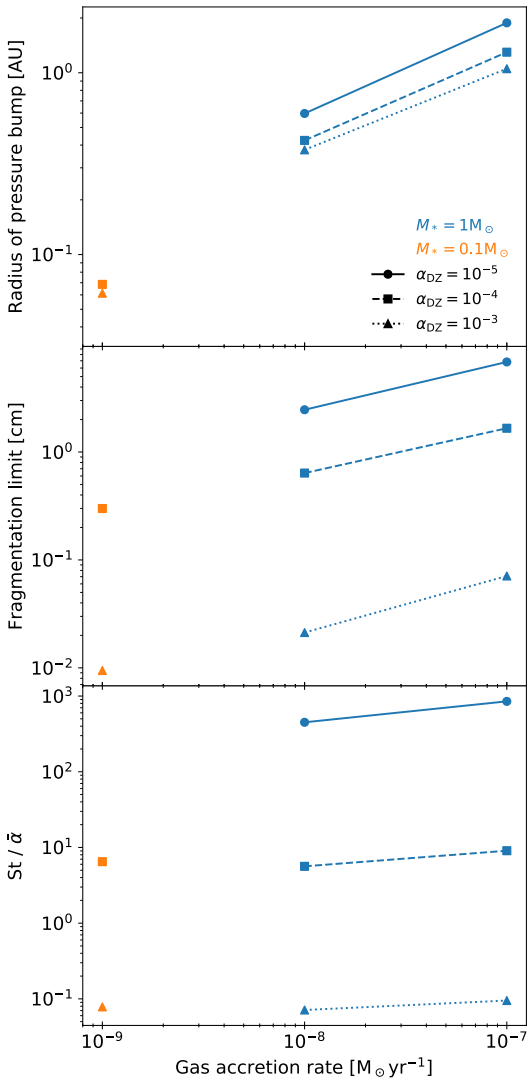

Figure 9. Radius of the pressure bump (top), maximum dust grain size (middle) and ratio of the Stokes number to the viscosity parameter ($\mathrm{St}/\bar{\alpha}$) at the pressure bump (bottom) as functions of the gas accretion rate, for a maximum dust grain size that corresponds to the grain growth limit due to turbulent fragmentation. Solid, dashed and dotted lines correspond to different values of the dead-zone viscosity parameter α_{DZ} as shown in the plot legend. The dust grain size and $\mathrm{St}/\bar{\alpha}$ are highly sensitive to the dead-zone viscosity parameter α_{DZ}. Conversely, varying α_{DZ} affects the location of the pressure bump only weakly. Blue lines show the results for a stellar mass $M_* = 1\,\mathrm{M}_\odot$, orange lines for $M_* = 0.1\,\mathrm{M}_\odot$. There is no solution for $M_* = 1\,\mathrm{M}_\odot$ and accretion rate of $\dot{M} = 10^{-9}\,\mathrm{M}_\odot\,\mathrm{yr}^{-1}$, nor for $M_* = 0.1\,\mathrm{M}_\odot$ and $\dot{M} \leqslant 10^{-10}\,\mathrm{M}_\odot\,\mathrm{yr}^{-1}$. See Sections 5.1 and 5.2.

maximum. The viscosity parameter $\bar{\alpha}$ at the pressure maximum is determined by the accretion through the dead zone at disc midplane and the accretion through an X-ray ionized layer high above the midplane. The former dominates since the density at midplane is much higher, and so $\bar{\alpha} \sim \alpha_{\mathrm{DZ}}$. Therefore, $\mathrm{St}_{\mathrm{frag}}/\bar{\alpha} \propto 1/\alpha_{\mathrm{DZ}}^2$.

Furthermore, the temperature at the pressure maximum is expected to be roughly $\sim$ 1000 K, as above this temperature thermionic and ion emission from dust grains lead to a sharp increase in the ionization fraction and the onset of the MRI at the disc midplane. However, the exact value varies as a function of dust grain properties, gas density at the pressure maximum, as well as the highly non-linear MRI criteria. The dependence of $\mathrm{St}_{\mathrm{frag}}/\bar{\alpha}$ on $\dot{M}$ comes mostly from the variations in this critical temperature, and to a lesser degree from the deviation of $\bar{\alpha}$ from α_{DZ}.

Overall, whether the dust grains become trapped in the pressure maximum depends on an assumed value of α_{DZ}. We may consider how the disc might evolve forward, depending on this value. First, if the dead-zone viscosity parameter is low, $\alpha_{\mathrm{DZ}} = 10^{-5}$, $\mathrm{St}_{\mathrm{frag}}/\bar{\alpha} \gg 1$. In this case, dust grains could readily accumulate at the pressure maximum. This accumulation might lead to an unstable configuration, as an increase in the dust-to-gas ratio leads to an increase in $\bar{\alpha}$ at a given radius (see Fig. 3). As the dust-to-gas ratio would increase at the pressure maximum, and decrease either side, this could lead to an emergence of an additional minimum in $\bar{\alpha}$, and thus to a formation of an additional pressure trap. Time-dependent simulations are needed to examine further evolution of the disc.

Second, consider a case in which the dead-zone viscosity parameter is closer to the middle of the plausible range, $\alpha_{\mathrm{DZ}} = 10^{-4}$. For all considered gas accretion rates $\mathrm{St}_{\mathrm{frag}}/\bar{\alpha} \sim 1$. In this case, considered by Jankovic et al. (2019), the gas pressure maximum does not trap large amounts of dust. This is because $\bar{\alpha}$ increases inwards of the pressure maximum, and $\mathrm{St}_{\mathrm{frag}}$ decreases. This limits the radial width of the pressure trap. Dust advection with the accreting gas is not sufficient to remove the dust grains from the trap; however, the grains are also mixed radially by the turbulence. The dust-to-gas ratio at the pressure maximum is then limited by the corresponding radial diffusion term. Nevertheless, dust would still accumulate in the entire region interior to the pressure maximum, as in the highly-turbulent innermost region dust grains become small enough to couple to the gas, reducing the radial drift relative to the outer disc.

In this work, we also find that a higher dust-to-gas ratio yields a larger extent of the high-viscosity inner region (see Section 3.1.2). This is highly beneficial for planet formation in the inner disc, as it implies that the accumulation of dust is not only sustainable, but also leads to a radial expansion of the high-viscosity, high-turbulence region inside of which the dust accumulates. In particular, this expansion is beneficial for the growth of the small fragmentation-limited dust grains into larger, more rigid solid bodies, i.e., into planetesimals. Specifically, planetesimals may form out of small grains through a combination of the streaming instabilities (SI) and the gravitational instability (Youdin & Goodman 2005; Johansen & Youdin 2007; Bai & Stone 2010; Johansen et al. 2012; Simon et al. 2016, 2017; Schäfer et al. 2017). Under certain conditions, the SI leads to localized concentrations of dust grains susceptible to gravitational collapse. Jankovic et al. (2019) pointed out that this process is unlikely in the inner disc if the pressure (and the density) maximum is located at very short orbital distances, as too close to the star the tidal effect of the star prevents the gravitational collapse. Therefore, the shift of the pressure maximum to larger orbital distances due to the accumulation of dust could potentially help to overcome this barrier and form planetesimals.

Finally, if the dead-zone viscosity parameter is high, $\alpha_{\mathrm{DZ}} = 10^{-3}$, $\mathrm{St}_{\mathrm{frag}}/\bar{\alpha} \ll 1$. In this case, dust grains are so small and well-coupled to the gas that they are advected through the pressure maximum inwards. Dust may still accumulate interior to the pressure maximum, as a consequence of fragmentation in the innermost regions, as noted above. However, it is unlikely that this could lead to the formation of larger solid bodies. While the exact value of the

dead-zone viscosity is unimportant for the location of the pressure maximum (see Fig. 9 and Section 5.1), in this case the grains would likely be too small, too well-coupled to the gas to start the streaming instabilities (Carrera et al. 2015; Yang et al. 2017).

5.3 Limitations

In this work, we have assumed that the MRI-accreting inner disc is in an equilibrium, steady state. However, there are several processes whose further study requires to consider the time dependence of the disc structure.

First, even if variations in the dust properties are neglected, the steady-state MRI-accreting inner disc is unstable to surface density perturbations (Mohanty et al. 2018). At a fixed radius, the MRI-driven accretion rate decreases with an increasing surface density (as calculated using the steady-state models). Therefore, a perturbation in the disc surface density might lead out of the steady-state, creating a pile up of mass in a certain region. This so-called viscous instability (Lightman & Eardley 1974; Pringle 1981) could have important consequences for the inner disc structure and planet formation, as it is likely to produce rings and gaps on the viscous timescale.

Second, the results presented in this work show that the accumulation of dust in the inner disc is possibly a highly dynamical process. The dust grain size and the dust-to-gas ratio strongly affect the MRI-driven viscosity at a given radius, and, concurrently, the extent of the innermost region within which the dust may accumulate. The evolution of the disc is particularly unclear if the dust is trapped in the pressure maximum, e.g., whether further evolution of gas and dust might lead to a modified equilibrium state, or creation of multiple viscosity minima (and pressure maxima).

Third, while we considered the effects of dust on the disc thermal and chemical structure, we did not account for the dynamical effects. If dust grains drift radially due to gas drag, there is also a back-reaction on the gas (Nakagawa et al. 1986). This becomes increasingly important at high dust-to-gas ratios. In particular, drag back-reaction acts to flatten the radial gas pressure profile, and so it would affect accumulation of dust in the pressure maximum (Taki et al. 2016). Further study of the early stages of planet formation in the inner disc should account for the self-consistent, time-dependent evolution of the gas and the dust.

Furthermore, it was shown that for some disc parameters dust growth could lead to steady-state solutions in which the disc is primarily ionized by stellar X-rays and no pressure maximum would exist. This deserves further study through time-dependent simulations, and also using a more detailed chemical network than considered here. In the regime in which the high-temperature effects are unimportant, at low dust-to-gas ratios (equivalent to larger grain sizes) simplified chemical networks overestimate the disc ionization levels, and the MRI-driven accretion efficiency, compared to the more complex networks (Ilgner & Nelson 2006).

Finally, the radiative properties of the disc are determined only by dust in this work. In the optically-thick regions (such as the disc midplane in our models), this is a good assumption since the Rosseland-mean opacity of the gas is always negligible compared to that of the dust where the pressure maximum is located. However, in the optically-thin regions (in the disc upper layers), Planck-mean opacity of the gas at high temperatures is comparable to that of micron-sized dust, and the absorption coefficient $\kappa_{\rm P}^{*}$ greatly exceeds that of cm-sized dust (e.g. Malygin et al. 2014). Since the gas accretes primarily through the dense, optically-thick regions around the disc midplane, we can expect that including the gas opacities would not change our results, as the higher absorption of stellar light would only increase the temperature in the uppermost disc layers. Nevertheless, note that the gas opacities are strongly non-monotonic, and the upper disc layers might not be in thermal equilibrium (Malygin et al. 2014), which is assumed to be the case here.

6 SUMMARY

We have explored how the structure of the MRI-accreting inner regions of protoplanetary discs changes as a function of the dust-to-gas ratio, dust grain size, and other disc and stellar parameters. We have especially focused on the location of the gas pressure maximum arising at the boundary between the highly-viscous innermost region and the low-viscosity outer region. The existence and the location of the pressure maximum, and the disc structure in its vicinity, are key to the formation of the super-Earths inside the water ice line.

At fixed dust parameters, the radius of the pressure maximum is directly related to the stellar mass M_{*} and the gas accretion rate $\dot{M}$. This is because the stellar mass and the accretion rate determine the total viscous dissipation at a given radius, and thus the temperature and the ionization fraction at disc midplane. The radius of the pressure maximum is inversely related to the assumed viscosity parameter in the MRI-dead zone $\alpha_{\rm DZ}$. The location of the pressure maximum corresponds to a minimum in the viscosity parameter. Even though in our model there is an MRI-active layer at all radii, in the outer regions this is a (X-ray ionized) layer high above the disc midplane (in the vicinity of the pressure maximum), and the disc primarily accretes through the dense MRI-dead regions around the midplane. Therefore, the minimum viscosity parameter is close in value to the dead-zone $\alpha_{\rm DZ}$.

However, this picture of the highly-viscous innermost region and the low-viscosity outer region changes qualitatively for some disc and stellar parameters. Specifically, for low gas accretion rates ($\leqslant 10^{-9}\,{\rm M}_{\odot}\,{\rm yr}^{-1}$), we find that steady-state solutions could exist in which there is no gas pressure maximum. In these solutions the disc features low gas surface densities and high viscosity driven by X-ray ionization. Such solutions are more likely to exist for larger grain sizes (and, equivalently, at lower dust-to-gas ratios).

At fixed stellar and disc parameters, as long as the pressure maximum does exist, its location moves radially outwards as the dust grains grow to $a_{\rm max} \sim 10^{-2}\,{\rm cm}$. Grain growth to still larger sizes results in the pressure maximum moving inwards, towards the star. This behaviour is primarily driven by the effects of dust opacities on the disc thermal structure.

We calculate the location of the pressure maximum for the case of dust growth being limited by turbulent fragmentation. For a Solar-mass star and gas accretion rates in the range $10^{-8}-10^{-7}\,{\rm M}_{\odot}\,{\rm yr}^{-1}$, this always places the pressure maximum outwards of 0.1 AU. In this fragmentation-limited regime, the radius of the pressure maximum depends very weakly on the dead-zone viscosity parameter, and it is most sensitive to the gas accretion rate. No pressure maximum exists for a Solar-mass star and a gas accretion rate of $\leqslant 10^{-9}\,{\rm M}_{\odot}\,{\rm yr}^{-1}$, nor for a stellar mass of $0.1\,{\rm M}_{\odot}$ for gas accretion rates $\leqslant 10^{-10}\,{\rm M}_{\odot}\,{\rm yr}^{-1}$. This suggests that planet formation in the inner disc is more likely early in the disc lifetime.

The fragmentation-limited dust grain size and its Stokes number are most sensitive to the value of the viscosity (and turbulence) parameter at the pressure maximum. As noted above, this roughly equals the assumed value of the viscosity parameter in the MRI-dead zone ($\alpha_{\rm DZ}$). Therefore, whether the dust grains can become

trapped in the pressure maximum is determined by this uncertain parameter. Dust trapping is likely for the lower end of plausible values ($\alpha_{\rm DZ} = 10^{-5}$) and will not happen for the higher end ($\alpha_{\rm DZ} = 10^{-3}$).

Importantly, the pressure maximum does not move inwards for higher dust-to-gas ratios. That is, dust accumulation near the pressure maximum (and/or inwards of it) should result in an expansion of the dust-enriched region. However, time-dependent simulations are needed to further study the potential outcomes, and the viability of planetesimal formation in the inner disc.

ACKNOWLEDGEMENTS

We thank Richard Booth, Thomas Haworth, Zhaohuan Zhu, Steven Desch, Neal Turner and Colin McNally for helpful discussions. M.R.J. acknowledges support from the President's PhD scholarship of the Imperial College London and the UK Science and Technology research Council (STFC) via the consolidated grant ST/S000623/1. JEO is supported by a Royal Society University Research Fellowship. This work was supported by an ERC-STG-2019 grant (PEVAP).

DATA AVAILABILITY

The data underlying this article will be shared on reasonable request to the corresponding author.

REFERENCES

Alcalá J. M., et al., 2014, A&A, 561, A2
Alcalá J. M., et al., 2017, A&A, 600, A20
Bai X.-N., Goodman J., 2009, ApJ, 701, 737
Bai X.-N., Stone J. M., 2010, ApJ, 722, 1437
Bai X.-N., Stone J. M., 2011, ApJ, 736, 144
Balbus S. A., Hawley J. F., 1991, ApJ, 376, 214
Baraffe I., Homeier D., Allard F., Chabrier G., 2015, A&A, 577, A42
Beitz E., Güttler C., Blum J., Meisner T., Teiser J., Wurm G., 2011, ApJ, 736, 34
Birnstiel T., Dullemond C. P., Brauer F., 2009, A&A, 503, L5
Birnstiel T., Dullemond C. P., Brauer F., 2010, A&A, 513, A79
Birnstiel T., Klahr H., Ercolano B., 2012, A&A, 539, A148
Bitsch B., Raymond S. N., Izidoro A., 2019, A&A, 624, A109
Blum J., Münch M., 1993, Icarus, 106, 151
Boley A. C., Ford E. B., 2013, arXiv e-prints, p. arXiv:1306.0566
Bukhari Syed M., Blum J., Wahlberg Jansson K., Johansen A., 2017, ApJ, 834, 145
Carrera D., Johansen A., Davies M. B., 2015, A&A, 579, A43
Chatterjee S., Tan J. C., 2014, ApJ, 780, 53
Chiang E., Laughlin G., 2013, MNRAS, 431, 3444
Cossou C., Raymond S. N., Hersant F., Pierens A., 2014, A&A, 569, A56
Cuzzi J. N., Hogan R. C., 2003, Icarus, 164, 127
Demirci T., Krause C., Teiser J., Wurm G., 2019, A&A, 629, A66
Desch S. J., Turner N. J., 2015, ApJ, 811, 156
Draine B. T., 2003, ApJ, 598, 1017
Drazkowska J., Alibert Y., Moore B., 2016, A&A, 594, A105
Dressing C. D., Charbonneau D., 2013, ApJ, 767, 95
Dressing C. D., Charbonneau D., 2015, ApJ, 807, 45
Dzyurkevich N., Flock M., Turner N. J., Klahr H., Henning T., 2010, Astronomy and Astrophysics, 515, A70
Fressin F., et al., 2013, ApJ, 766, 81
Gammie C. F., 1996, ApJ, 457, 355
Hansen B. M. S., Murray N., 2013, ApJ, 775, 53
Hsu D. C., Ford E. B., Ragozzine D., Ashby K., 2019, AJ, 158, 109
Hu X., Tan J. C., Zhu Z., Chatterjee S., Birnstiel T., Youdin A. N., Mohanty S., 2018, ApJ, 857, 20
Ilgner M., Nelson R. P., 2006, A&A, 445, 205
Izidoro A., Ogihara M., Raymond S. N., Morbidelli A., Pierens A., Bitsch B., Cossou C., Hersant F., 2017, MNRAS, 470, 1750
Izidoro A., Bitsch B., Raymond S. N., Johansen A., Morbidelli A., Lambrechts M., Jacobson S. A., 2019, arXiv e-prints, p. arXiv:1902.08772
Jacquet E., Gounelle M., Fromang S., 2012, Icarus, 220, 162
Jankovic M. R., Owen J. E., Mohanty S., 2019, MNRAS, 484, 2296
Johansen A., Youdin A., 2007, ApJ, 662, 627
Johansen A., Youdin A. N., Lithwick Y., 2012, A&A, 537, A125
Kretke K. A., Lin D. N. C., Garaud P., Turner N. J., 2009, ApJ, 690, 407
Lightman A. P., Eardley D. M., 1974, ApJ, 187, L1
Malygin M. G., Kuiper R., Klahr H., Dullemond C. P., Henning T., 2014, A&A, 568, A91
Manara C. F., Robberto M., Da Rio N., Lodato G., Hillenbrand L. A., Stassun K. G., Soderblom D. R., 2012, ApJ, 755, 154
Manara C. F., et al., 2017, A&A, 604, A127
Mathis J. S., Rumpl W., Nordsieck K. H., 1977, ApJ, 217, 425
McNeil D. S., Nelson R. P., 2010, MNRAS, 401, 1691
Mohanty S., Jayawardhana R., Basri G., 2005, ApJ, 626, 498
Mohanty S., Ercolano B., Turner N. J., 2013, ApJ, 764, 65
Mohanty S., Jankovic M. R., Tan J. C., Owen J. E., 2018, ApJ, 861, 144
Mulders G. D., Pascucci I., Apai D., Ciesla F. J., 2018, AJ, 156, 24
Nakagawa Y., Sekiya M., Hayashi C., 1986, Icarus, 67, 375
Ogihara M., Ida S., 2009, ApJ, 699, 824
Ormel C. W., Cuzzi J. N., 2007, A&A, 466, 413
Owen J. E., Wu Y., 2017, ApJ, 847, 29
Perez-Becker D., Chiang E., 2011, ApJ, 735, 8
Pollack J. B., Hollenbach D., Beckwith S., Simonelli D. P., Roush T., Fong W., 1994, ApJ, 421, 615
Pringle J. E., 1981, ARA&A, 19, 137
Raymond S. N., Cossou C., 2014, MNRAS, 440, L11
Raymond S. N., Barnes R., Mandell A. M., 2008, MNRAS, 384, 663
Salmeron R., Wardle M., 2008, MNRAS, 388, 1223
Sano T., Miyama S. M., Umebayashi T., Nakano T., 2000, ApJ, 543, 486
Schäfer U., Yang C.-C., Johansen A., 2017, A&A, 597, A69
Schlichting H. E., 2014, ApJ, 795, L15
Schräpler R., Blum J., Seizinger A., Kley W., 2012, ApJ, 758, 35
Shakura N. I., Sunyaev R. A., 1973, A&A, 500, 33
Simon J. B., Armitage P. J., Li R., Youdin A. N., 2016, ApJ, 822, 55
Simon J. B., Armitage P. J., Youdin A. N., Li R., 2017, ApJ, 847, L12
Taki T., Fujimoto M., Ida S., 2016, A&A, 591, A86
Terquem C., Papaloizou J. C. B., 2007, ApJ, 654, 1110
Van Eylen V., Agentoft C., Lundkvist M. S., Kjeldsen H., Owen J. E., Fulton B. J., Petigura E., Snellen I., 2018, MNRAS, 479, 4786
Wardle M., 2007, Ap&SS, 311, 35
Weidenschilling S. J., 1977, MNRAS, 180, 57
Wu Y., 2019, ApJ, 874, 91
Yang C.-C., Johansen A., Carrera D., 2017, A&A, 606, A80
Youdin A. N., Goodman J., 2005, ApJ, 620, 459

This paper has been typeset from a TEX/LATEX file prepared by the author.